Refined Fiber Laser Model

Will Ray,[1,2] Kurt Wiesenfeld,[2] and Jeffrey L. Rogers[1]

[1]*HRL Laboratories, LLC, Malibu CA 90265*

[2]*Center for Nonlinear Science and School of Physics, Georgia Institute of Technology, Atlanta GA 30332*

(Dated: November 10, 2007)

Abstract

We refine dynamical equations derived to explain recently reported coherence effects in fiber laser arrays by extending the range of validity to include both three-level and four-level lasers. Predicted features of the model, including transitions between distinct dynamical states, are evaluated against both published experiments from other investigators and new experiments we performed. The comparisons demonstrate excellent agreement over a wide range of operating conditions.

I. INTRODUCTION

As lasers and nonlinear dynamics have simultaneously undergone periods of discovery and maturation each has contributed to a better understanding of the other. While many of the diverse behaviors and instabilities present in lasers were identified early in their discovery, this richness was not widely recognized until Haken mapped semiclassical optical equations onto those describing convective fluid flow [1]. Even though this mapping was restricted in scope for each of these dynamical systems the connection to fluids, where instabilities and transitions through a range of behaviors were well accepted, was enough to stimulate broader interest in optical instabilities. As these areas matured the understanding developed provided a basis for several optical technologies. Examples include encryption without key distribution [2–4], dynamical control [5], sensitive structural damage detection [6, 7], and synchronization of small numbers of lasers [8–11]. Conversely, lasers offer precise control over initial conditions, measurement capability, and short laboratory transient times, making them an attractive resource for probing fundamentals of nonlinear dynamics [12–15].

Dynamical networked systems are a topic of active investigation in nonlinear sciences where another period of scientific and technological development can occur in conjunction with lasers. A particular optics example relevant to studies of network dynamics is the production of coherent radiation from a laser array. Due to the technological possibilities an array where all the lasers have the same frequency and relative phase (inphase state) is a longstanding goal [16]. However, producing stable ordered arrays has also proved elusive. Recent fiber laser experiments have provided renewed optimism for success with arrays having as many as 9 coherent lasers and output powers up to a few hundred watts [17]. Current attempts to extend to larger arrays and higher powers have failed.

Making further progress will require a better understanding of the physical mechanisms involved in stable coherent emission. While there have been a number of similarly successful experiments with a few lasers [18–22], there have also been almost as many explanations presented [20–24]. So far, consensus has been difficult to achieve. One of the original promising experiments [17] was based on general notions from nonlinear dynamics. To gain a better understanding of this class of systems a model of nonlinear iterative maps was introduced [25]. Despite being relatively simple this model correctly captures qualitative features observed in some lasers. It is also an attractive option for investigating large arrays

since computations on the iterative maps are much faster than flow descriptions which may be stiff. However, if this model is going to be relevant in deducing physical mechanisms underlying laser array behavior it is necessary that it correctly captures well-understood dynamical results of a single laser. For these purposes it makes sense to consider the array size limit of a single laser. The model should additionally encompass the broad range of elemental laser sources that have successfully demonstrated stable coherent emission.

This paper extends the iterative map model and compares it to previously published experiments and new experiments. For a single laser we find two distinct reports with sufficient laboratory details to carry out meaningful comparisons. One of these papers [26] reports regions of stable continuous wave (cw) and self-pulsing states in a single three-level Er-doped fiber laser with high cavity losses. The other investigates a single four-level Nd:glass laser with low cavity losses [27]. Finally, we augment these experiments with our own laboratory investigations of four-level Nd lasers with high cavity losses. Collectively, these experiments cover a wide range of gain types and loss characteristics. Using our refined model we find quantitative agreement with all these experiments. In the low loss case, the modified theory effectively reduces to the original model; however, when high losses are present the refinements are essential to achieving full quantitative agreement.

II. THEORETICAL MODEL

We consider a linear laser cavity composed of a perfect mirror or reflector at one end, gain media and passive waveguides, and a partially reflective output face. In particular, the experiments we will compare with involve lasers constructed from a rare-earth doped fiber capped by a fiber Bragg grating or mirror with nearly perfect reflectivity (99%) on one end and an output facet with lower reflectivity on the other end. This linear cavity may be lengthened by insertion of passive fiber between either end mirror and the doped fiber.

In Ref. [25] an iterative map model was derived for the dynamical evolution of an array of fibers. For a single fiber operating on a single longitudinal mode, these equations reduce to:

$$E' = re^{G+i\phi}E + \eta \tag{1}$$

$$G' = G + \epsilon\left[G^p - G - \frac{1}{I_{SAT}}\left(1 - e^{-2G}\right)|E|^2\right]. \tag{2}$$

Here, the dynamical variables are the complex electric field E and real gain G. The prime denotes updated values after one cavity round trip time T. The parameters are the output field reflectivity r, the pump strength G^p, and the ratio of round trip time to fluorescence time $\epsilon = T/\tau$. The pump strength is written in units of gain and acts as a stress parameter. The phase ϕ contains the free-propagation phase accumulated over one round trip and I_{SAT} is the saturation intensity of the laser. Finally, η is a noise term modeling spontaneous emission and other sources.

Our refinement of the model stems from a more detailed consideration of the gain medium. As a result Eq. (2) takes on a different form for three- and four-level lasers. The full derivations make use of the standard Rigrod analysis for two-way fibers [28] and closely follow the steps of Ref. [25].

In Ref. [25], the evolution of the gain variable is derived starting from the partial differential equations

$$\frac{\partial I^+}{\partial z} = N\sigma I^+ \tag{3}$$

$$\frac{\partial I^-}{\partial z} = -N\sigma I^- \quad \text{and} \tag{4}$$

$$\frac{\partial N}{\partial t} = R^p - \frac{N}{\tau} - \frac{\sigma}{\hbar\omega} N \left[I^+ + I^-\right] \tag{5}$$

where $I^+(z,t)$ is the intensity of the forward-propagating electromagnetic wave, $I^-(z,t)$ the corresponding backward-propagating quantity, and $N(z,t)$ the number of inverted atoms per unit length; σ is the stimulated emission cross-section, and $R^p(z,t)$ the pump rate parameter. The gain variable is directly proportional to the population inversion $N(z,t)$ integrated over the length of the gain medium. A more refined model follows from considering the atomic-level dynamics in greater detail.

Three-level Laser

Consider first a three-level scheme [Fig. 1(a)]. The external pump elevates atoms from the ground state g to an upper pump band u. This pump band rapidly relaxes to the meta-stable upper lasing level 2. Atoms in the upper lasing level then decay to the ground state via fluorescence and stimulated emission from photons in the cavity. The ground state serves as the lower lasing level. The dynamics of this process is described by replacing the single rate equation (5) by the following set of three rate equations:

$$\frac{\partial N_u}{\partial t} = W^p (N_g - N_u) - \frac{N_u}{\tau_u} \tag{6}$$

$$\frac{\partial N_2}{\partial t} = \frac{N_u}{\tau_u} - \frac{N_2}{\tau} - \frac{\sigma}{\hbar\omega} (N_2 - N_g) \left[I^+ + I^-\right] \tag{7}$$

$$\frac{\partial N_g}{\partial t} = \frac{N_2}{\tau} + \frac{\sigma}{\hbar\omega} (N_2 - N_g) \left[I^+ + I^-\right] - W^p (N_g - N_u), \tag{8}$$

where $N_x(z,t)$ is the population of atoms per unit length in energy level x, τ_u is the relaxation time from the pump band to the upper lasing level, fluorescence occurs between the upper and lower lasing levels with a characteristic time τ, and W^p is the pumping transition rate. The atomic gain is proportional to the amount of population inversion $N(z,t)$, with the latter given by

$$N = N_2 - N_g. \tag{9}$$

The evolution of N is deduced by assuming that the relaxation time of the lasing transition τ is much slower than τ_u. Then N_u may be adiabatically eliminated; moreover, the fast decay from this level essentially puts all the atoms in either the upper lasing level or the ground state, so $N_u \simeq 0$ and the conserved total number of atoms N_{tot} is

$$N_{\rm tot} = N_g + N_2. \tag{10}$$

Under these conditions, one can show that the rate equation for the population inversion reduces to

$$\frac{\partial N}{\partial t} = 2W^p N_g - \frac{2N_2}{\tau} - \frac{2\sigma}{\hbar\omega} (N_2 - N_g) \left[I^+ + I^-\right]. \tag{11}$$

The terms on the righthand side of Eq.(11) may be rewritten in terms of N and N_{tot} instead of N_2 and N_g. Starting from the set of partial differential equations, (3), (4), and (11), it is a straightforward matter to repeat the steps carried out in Ref. [25] to arrive at the corresponding iterative map model. One finds

$$G' = G + \epsilon \left[W^p \tau (G_{\rm tot} - G) - (G_{\rm tot} + G)\right] - \frac{2\epsilon}{I_{\rm sat}} \left(1 - e^{-2G}\right) |E|^2, \tag{12}$$

where

$$G = \sigma \int_0^L N(z,t) dz \tag{13}$$

and

$$I_{\rm sat} = \frac{\hbar\omega}{\sigma\tau}. \tag{14}$$

Four-level Laser

Consider next a four-level scheme [Fig. 1(b)]. Atoms from the ground state g are elevated to an upper pump band u before rapidly decaying to the meta-stable upper lasing level 2. Here the lasing transition occurs between the upper lasing level and the lower lasing level 1. Atoms in the lower lasing level then decay quickly to the ground state. This scenario is regulated by the following set of four rate equations:

$$\frac{\partial N_u}{\partial t} = W^p (N_g - N_u) - \frac{N_u}{\tau_u} \tag{15}$$

$$\frac{\partial N_2}{\partial t} = \frac{N_u}{\tau_u} - \frac{N_2}{\tau} - \frac{\sigma}{\hbar\omega} (N_2 - N_1) \left[I^+ + I^-\right] \tag{16}$$

$$\frac{\partial N_1}{\partial t} = \frac{N_2}{\tau} + \frac{\sigma}{\hbar\omega} (N_2 - N_1) \left[I^+ + I^-\right] - \frac{N_1}{\tau_1} \tag{17}$$

$$\frac{\partial N_g}{\partial t} = \frac{N_1}{\tau_1} - W^p (N_g - N_u). \tag{18}$$

The parameters are the same as those in the three-level lasing scheme with τ_1 defined as the relaxation time from the lower lasing level to the ground state. The population inversion $N(z,t)$ is given by

$$N = N_2 - N_1. \tag{19}$$

Since τ_u and τ_1 are much faster than the fluorescence time between the upper and lower lasing levels, N_u and N_1 may be adiabatically eliminated as before, and again the conserved total number of atoms $N_{tot}(z,t)$ is

$$N_{\rm tot} = N_g + N_2.$$

The resulting equation for the population inversion is found to be

$$\frac{\partial N}{\partial t} = W^p (N_{\rm tot} - N) - \frac{N}{\tau} - \frac{\sigma}{\hbar\omega} N \left[I^+ + I^-\right]. \tag{20}$$

Equation (20) replaces Eq. (5) as the starting point for the Rigrod analysis. If only a small fraction of the available atoms are excited then $N_{tot} >> N$ and we recover the original model given in Eq. (5). Repeating the steps of Ref. [25], we arrive at the iterative map for the gain field of a 4-level laser

$$G' = G + \epsilon \left[W^p \tau (G_{\rm tot} - G) - G\right] - \frac{\epsilon}{I_{\rm sat}} \left(1 - e^{-2G}\right) |E|^2. \tag{21}$$

III. ANALYSIS

Analyzing the refined model we predict parameter ranges over which cw emission is stable for each lasing scheme. Analytic calculations of the transient relaxations to the cw state allow us to make empirical estimates of the model parameters. To facilitate comparison with experiments, it is convenient to recast the pumping rate W^p in terms of a relative pump rate x defined as

$$x = \frac{W^p}{W^p_{th}}, \tag{22}$$

where W^p_{th} represents the pump rate at lasing threshold.

A. 3-level lasers

The dynamical evolution of the iterative map model for a single laser operating in a three-level lasing scheme is given by

$$E' = re^{G+i\phi}E + \eta \tag{23}$$

$$G' = G + \epsilon\left[xW^p_{th}\tau\left(G_{tot} - G\right) - \left(G_{tot} + G\right) - \frac{2}{I_{sat}}\left(1 - e^{-2G}\right)|E|^2\right]. \tag{24}$$

The noise-free system admits two fixed point solutions. Writing these in terms of intensity $I = |E|^2$ yields

$$\tilde{I} = 0 \qquad , \qquad \tilde{G} = G_{tot}\frac{xW^p_{th}\tau - 1}{xW^p_{th}\tau + 1} \tag{25}$$

and

$$\tilde{I} = I_{SAT}\frac{(x-1)\left(G_{tot} + \ln\left(\frac{1}{r}\right)\right)}{2\left(1 - r^2\right)} \qquad , \qquad \tilde{G} = \ln\left(\frac{1}{r}\right). \tag{26}$$

Physically, Eq. (25) is the off state [Fig. 2(a)] and Eq. (26) is cw emission [Fig. 2(b)]. In the off state output losses are greater than gain. The phase portrait in Fig. 2(a) shows the system trajectory decaying rapidly to a flashlight cavity and only amplified spontaneous emission is observed. A bifurcation occurs at lasing threshold ($x = 1$) and the stability of the off state and cw are swapped as the relative pump rate is increased past unity. The pump rate at threshold expressed in terms of the system parameters is

$$W^p_{th}\tau = \frac{G_{tot} + \ln\left(\frac{1}{r}\right)}{G_{tot} - \ln\left(\frac{1}{r}\right)}. \tag{27}$$

At pump rates higher than threshold, the intensity rises according to Eq. (26) with a slope efficiency

$$\frac{d\tilde{I}}{dW^p} = I_{SAT}\tau \frac{G_{tot} - \ln\left(\frac{1}{r}\right)}{2\left(1-r^2\right)}. \tag{28}$$

The stability of the cw state may be assessed by examining the eigenvalues of the associated Jacobian matrix

$$\lambda_{1,2} = 1 - \frac{\epsilon}{2}\left(1 + W^p\tau + 4r^2\tilde{I}\right) \pm \sqrt{\frac{\epsilon^2}{4}\left(1 + W^p\tau + 4r^2\tilde{I}\right)^2 - 4\epsilon\left(1-r^2\right)\tilde{I}} \tag{29}$$

evaluated at the fixed point solution. Unless x lies slightly above lasing threshold, the discriminant in Eq. (29) is negative and the eigenvalues are complex. The magnitude of the eigenvalues in the cw state are found to be less than one until the relative pump rate reaches

$$x_H = \frac{1 + 2\left(G_{tot} + \ln\left(\frac{1}{r}\right)\right)\frac{1-2r^2}{1-r^2}}{2\left(G_{tot} + \ln\left(\frac{1}{r}\right)\right)\frac{1-2r^2}{1-r^2} - \frac{G_{tot}+\ln\left(\frac{1}{r}\right)}{G_{tot}-\ln\left(\frac{1}{r}\right)}}. \tag{30}$$

For $x > x_H$ the **remove** *system* cw fixed point is no longer attracting due to a Hopf bifurcation at x_H. Instead the dynamics of both the gain and intensity are attracted to a limit cycle [Fig. 2(c)]. Simulations of the system show that as x is increased further the oscillations appear as a regular pulse train with a repetition rate that increases in a linear fashion with the pump. The height of an individual pulse grows while the pulse width shrinks; in addition, the regularity of the pulses eventually dissolves into more complicated patterns.

Emission in the cw state is stable for relative pump rates in the interval $1 < x < x_H$. Unlike the original iterative map description [25], this interval is not a function of r alone.

Finally it is worthwhile to examine the transient characteristics of the system variables in cw state when they are perturbed away from their fixed point values. As portrayed in Fig. 2(b), the intensity and gain dynamics exhibit a ring-down back to their steady state values at a characteristic frequency and decay rate. These properties are determined by the eigenvalues of the Jacobian matrix

$$\lambda_{1,2} = 1 - \Gamma_{RO}T \pm i\omega_{RO}T. \tag{31}$$

The real and imaginary parts of the eigenvalues represent the decay rate Γ_{RO} and the frequency ω_{RO} of these relaxation oscillations. Comparing Eq. (31) with Eq. (29) we identify

the decay rate of the oscillations as

$$\Gamma_{RO} = \frac{1}{2\tau_{fl}}\left[1 - \frac{r^2\left(G_{tot} + \ln\left(\frac{1}{r}\right)\right)}{1-r^2} + x\left(\frac{G_{tot} + \ln\left(\frac{1}{r}\right)}{G_{tot} - \ln\left(\frac{1}{r}\right)} + \frac{r^2\left(G_{tot} + \ln\left(\frac{1}{r}\right)\right)}{1-r^2}\right)\right], \tag{32}$$

while the frequency is

$$\omega_{RO}^2 = \frac{2(x-1)\left(G_{tot} + \ln\left(\frac{1}{r}\right)\right)}{T\tau_{fl}} - \Gamma_{RO}^2. \tag{33}$$

Since the first term in Eq. (33) is typically orders of magnitude larger than the second, the frequency is well approximated by

$$\omega_{RO}^2 = \frac{2(x-1)\left(G_{tot} + \ln\left(\frac{1}{r}\right)\right)}{T\tau_{fl}}, \tag{34}$$

i.e. the geometric mean of the decay rates of the cavity and the population inversion. Since static and dynamic quantities may be carefully measured in an experiment over a range of pumping strengths, system parameters may be estimated using a combination of the above expressions.

B. 4-level lasers

For a single four-level laser the refined model is given by

$$E' = re^{G+i\phi}E + \eta \tag{35}$$

$$G' = G + \epsilon\left[xW_{th}^p\tau(G_{tot} - G) - G - \frac{1}{I_{SAT}}(1 - e^{-2G})|E^2|\right]. \tag{36}$$

Again, two fixed point solutions exist:

$$\tilde{I} = 0, \qquad \tilde{G} = G_{tot}\frac{xW_{th}^p\tau}{xW_{th}^p\tau + 1}. \tag{37}$$

and

$$\tilde{I} = I_{SAT}\frac{(x-1)\ln\left(\frac{1}{r}\right)}{1-r^2} \qquad , \qquad \tilde{G} = \ln\left(\frac{1}{r}\right). \tag{38}$$

Physically, Eq. 37 is the off state and Eq. 38 is cw emission. In this lasing scheme the pump rate at threshold is

$$W_{th}^p\tau = \frac{\ln\left(\frac{1}{r}\right)}{G_{tot} - \ln\left(\frac{1}{r}\right)}. \tag{39}$$

and the slope efficiency follows from Eq. (38) as

$$\frac{d\tilde{I}}{dW^p} = I_{SAT}\tau\frac{G_{tot} - \ln\left(\frac{1}{r}\right)}{1-r^2}. \tag{40}$$

A linear stability analysis shows that cw emission is stable in a range $1 < x < x_H$, where the Hopf bifurcation point x_H is now

$$x_H = \frac{1 + 2\ln(\frac{1}{r})\frac{1-2r^2}{1-r^2}}{2\ln(\frac{1}{r})\frac{1-2r^2}{1-r^2} - \frac{\ln\left(\frac{1}{r}\right)}{G_{tot}-\ln\left(\frac{1}{r}\right)}}. \tag{41}$$

As in the three-level iterative map description, the range of stable cw emission depends on both the cavity losses and the total linear gain.

The decay of the relaxation oscillations may be written as

$$\Gamma_{RO} = \frac{1}{2\tau_{fl}}\left[1 - \frac{r^2\ln(\frac{1}{r})}{1-r^2} + x\ln\left(\frac{1}{r}\right)\left(\frac{1}{G_{tot} - \ln\left(\frac{1}{r}\right)} + \frac{r^2}{1-r^2}\right)\right], \tag{42}$$

with an associated characteristic frequency approximated by

$$\omega_{RO}^2 = \frac{2(x-1)\ln(\frac{1}{r})}{T\tau_{fl}}. \tag{43}$$

IV. COMPARISON WITH EXPERIMENT

In the refined model, for a fixed pump rate, laser behavior is determined by cavity losses and total linear gain. For the purposes of improving model-experiment correspondence it is desirable to determine these parameters from laboratory measurements. In this section we conduct a quantitative comparison of our three-level model against an experimental study of an Er-doped fiber laser and our four-level model against two sets of experiments on Nd-doped fiber lasers in the limit of low and high cavity losses.

A. Three-level laser

In Ref. [26] dynamical behavior of a high-gain fiber laser with large cavity losses was systematically investigated in a series of experiments involving a number of cavity configurations. A longitudinally-pumped linear cavity was formed by placing high-reflecting mirrors (at the lasing wavelength) at both ends of erbium-doped fiber. Here we focus on three measurements of the output steady state intensity dynamics made at a constant input pump power for fiber lengths of 3 m, 4 m, and 4.5 m. For each fiber length Table I reproduces detailed estimates of light amplification, pump absorption, and cavity losses reported in

Table II of Ref. [26]. These parameters are derived from measurements of the relaxation oscillations and the turn-on time over a sweep of pump powers.

The system parameters reported in Ref. [26] are appropriate for a rate equation description of the system. The expressions in Table II provide a direct translation of these parameters to those in the iterative map model. The round-trip time T is derived from the cavity length assuming an index of refraction $\eta = 1.53$ in the doped fiber.

Using the relationships in Table II to approximate model parameters allows reported intensity dynamics to be compared with computations on our three-level model. To simulate the spontaneous emission in the fiber laser, a small amount of Langevin noise is added to real and imaginary parts of the electric field at each iteration. The standard deviation of the noise amplitude is set to 10^{-4}. This magnitude is consistent with what is expected from laboratory measurements and is typically used in rate equation descriptions for fiber laser systems.

For a 3 m fiber Ref. [26] reports cw output, reproduced in Fig. 3(a), at a pump power of $P = 400\ mW$ with small fluctuations due to dynamical and measurement noise. Experimental parameters listed in the first row of Table I yield model operating conditions: $r = 0.0892$, $\epsilon = 3.06 \times 10^{-6}$, $W^p = 3,136\ s^{-1}$, $\tau = 10\ ms$, and $G_{tot} = 2.82$. Since the reported experimental intensity dynamics are presented in arbitrary units, we are free to set $I_{sat} = 1$ and examine relative values in intensity.

In Fig. 3(b) we plot the simulated intensity time series of the three-level map [Eqs. (23-24)]. In agreement with the experimental results the intensity displays cw emission. The small oscillations present in the model are due to excited relaxation oscillations in response to the noise term.

To gain perspective on how close these operating conditions come to the pulsing regime, in Fig. 4(a) we plot the predicted phase diagram as a function of $\ln(r)$. Besides r and the pump (expressed as the relative pump rate x) the rest of the parameters remain fixed. The cross indicates the parameter values used to generate the time series shown in Fig. 3(b). This operating point lies well within the cw regime (white region) and it would take a significant change in the system, for instance an increase in r, to drive the dynamics into the pulsing state (gray region). The system is in an off state, represented by the cross-hatched region in Fig. 4(a), whenever the pump is below lasing threshold ($x < 1$) or the cavity losses correspond to a threshold gain greater than G_{tot}. The cw and pulsing regimes are separated

by the line formed from $x_H(r)$ defined by Eq. (30).

For the medium length fiber of 4 m and the same pump power the reported intensity measurements, reproduced in Fig. 3(c), show a train of eight pulses in a 200 μs window. The height of an individual pulse is roughly five times the level of the constant intensity measurement in the 3 m cavity. The second row in Table I allows us to define our model parameter values for the 4 m cavity: $r = 0.0457$, $\epsilon = 4.08 \times 10^{-6}$, $W^p = 2,848\ s^{-1}$, $\tau = 10\ ms$, and $G_{tot} = 3.75$.

The intensity dynamics computed from the model are plotted in Fig. 3(d). The 200 μs time trace shows a train of seven pulses with a height four times greater than the simulated intensity in Fig. 3(b) in quantitative agreement with the experimental time trace. The bifurcation diagram associated with these model parameters is shown in Fig. 4(b). Notice that the cw and pulsing regions are stretched to higher cavity losses (lower values of r). The extension of both regimes is a result of the increase of the total linear gain in the longer fiber. The cross denotes operating conditions of Fig. 3(d). This lies close to, but still below, the predicted line of Hopf bifurcations separating cw and pulsing regimes. Without noise, the system would exhibit cw emission as predicted by this diagram. The small amount of additive noise is sufficient to push the system into the pulsing state.

Finally, even larger pulses in the intensity dynamics were measured at the same input pump power when the cavity was extended to a fiber length of 4.5 m. The reported intensity dynamics are reproduced in Fig. 3(e), and a train of nine pulses now appear in a 200 μs window with heights that are ten times larger than the level of the constant intensity measurement in the 3 m cavity. Using Table I model parameters are found to be: $r = 0.0387$, $\epsilon = 4.59 \times 10^{-6}$, $W^p = 2,748\ s^{-1}$, $\tau = 10\ ms$, and $G_{tot} = 4.22$. A similar sequence of pulses is observed in the simulated intensity displayed in Fig. 3(f). Eight pulses appear in the time trace, reaching ten times higher than the simulated intensity in Fig. 3(b). These heights are even more irregular, a feature also apparent in the corresponding experimental intensity time trace. Similar to the experiment, the pulse widths are also narrower than the trace in Fig. 3(d). The phase diagram for these parameters is shown in Fig. 4(c). The cross denoting the operating conditions of Fig. 3(f) is placed well inside the pulsing regime.

The foregoing illustrates the predictive capability of the iterative map model for three-level lasing schemes. Once calibrated with experimentally derived parameters, the analytic calculation for the onset of pulsing accurately predicts the range of pump rates where cw

emission is stable. The transition from cw to pulsing emission for increasing fiber lengths can be understood as an imbalance between the effects of two parameters. The cavity losses are seen to increase for longer cavity lengths, pushing the system away from pulsing threshold. However, the growth in G_{tot} expands the stability of the pulsing regime at a faster rate, and a cross-over into the pulsing regime ensues. In addition, features of the simulated pulse dynamics, such as repetition rate and pulse height, show reasonable quantitative agreement with their experimental counterparts.

B. Four-level lasers

In the refinement of governing dynamical equations for four-level lasers, the inclusion of the total linear gain to the original set of iterative maps only affects the representation of the pumping term. As pointed out in Sec. II, this modification is significant only when considerable cavity losses are present. The original form of the equations [25] are appropriate when the laser suffers low or moderate cavity losses comprising only a small fraction of the total gain.

In view of this distinction, we compare the predictions of the four-level iterative map model to two experiments of a Nd:glass laser operating in the limit of low and high cavity losses, respectively.

1. Low Cavity Losses

Experiments reported in Ref. [27] studied temporal characteristics of the relaxation oscillations in five Nd-doped fiber lasers. Here we focus on the characterization of the intensity dynamics reported for the laser labeled *Lycom a*. In the experiments a segment of 750 mm active fiber is arranged in a linear cavity with a total length of 980 mm. One end of the fiber is coated with multiple dielectric layers to provide 99.5% reflection of the incident light, while the other end couples roughly 95% of the light back into the cavity. A slow photon decay rate $8.9 \times 10^6\ s^{-1}$ is reported for this laser as well as a fluorescence time of 460 μs.

Although a short fiber length providing limited gain is used in these experiments, the very low cavity losses yield a small threshold gain and it is estimated in Ref. [27] that the total linear gain is at least 40 times larger than the threshold level. Since $G_{tot} >> \tilde{G}$ the

original form of the iterative map model is adequate for evaluating the dynamics of this laser system. To characterize the parameters of this model, we use the reported photon decay rate to estimate $r = 0.957$. The fluorescence time and cavity length of this laser imply that $\epsilon = 2.17 \times 10^{-5}$.

In Fig. 5(a) we reproduce Fig. 4 from Ref. [27] displaying the experimental intensity time series after the pump is switched from off to a relative pump rate of 3.2 times the lasing threshold. The intensity is observed to ring down to a steady state level after spiking begins at 0.2 *ms*. Using the above parameters in Eqs. (1-2) with $G^p = 0.139$ and $G = 0$ when the pump is switched on, the simulated turn-on of the laser is shown in Fig. 5(b). The relaxation oscillation frequency and the turn on time at 0.2 *ms* show excellent agreement.

In these experiments, the intensity dynamics displayed only cw emission even up to the highest pump rates reported, some six times the lasing threshold. This is in agreement with our model. For these parameters simulations of Eqs. (1-2) imply that cw emission is stable for *any* pumping level above lasing threshold. To see this, note that the Hopf bifurcation curve $x_H(r)$ may be estimated from Eq. (41) omitting the term containing G_{tot}. The dashed line in Fig. 6 represents this curve as a function of the cavity losses. An analysis of Eq. (41) shows that for $r^2 > 0.5$, the Hopf bifurcation curve assumes values less than the threshold pump level and so only cw emission is predicted for all pump levels above lasing threshold. This asymptotic boundary to the onset of pulsing is denoted by the dotted line A_2 in Fig. 6.

The theoretical analysis together with the observation of cw emission in the experiment at high pump levels suggests that many lasers with very low cavity losses share this feature [29]. It may be that other low-loss fiber lasers could show pulsing behavior. If so, there would have to be some physical mechanism involved that is not taken into account in our model.

2. High Cavity Losses

We now consider a four-level fiber laser with significant cavity losses. Such fibers were previously used as an elemental source in laser array experiments [22]. In this case we expect that the modified form of the model given by Eqs. (35-36) is necessary to capture the observed dynamics.

We performed experiments using a linear cavity arrangement composed of 14 m of fiber including 6 m of Nd-doped fiber between two passive sections. A fiber Bragg grating on one

end provides nearly 100% reflection while a flat-cleave on the other cavity end retains less than 4% of the incident intensity. While heavy losses occur at the output facet, considerable internal losses are present as well. We estimate that less than 5% of the generated intensity emerges out of the laser. The internal losses are primarily attributed to numerous splices along the cavity length, in particular at the connections between the passive and active fibers with disparate numerical apertures.

Although substantial cavity losses are already present in this system, we induced additional losses to examine the consequence on the output light dynamics. At multiple locations along the length of the cavity, tightly wound coils of passive fiber are iteratively compressed to provide a wide range of applied cavity losses. To gather an estimate of the cavity losses, at each loss level the frequency of the relaxation oscillations is recorded over a large sweep of the pump. In Fig. 7(a) relaxation oscillation measurements for two levels of cavity losses are plotted for increasing relative pump rates. Using the known fluorescence time of 460 μs for Nd:glass and fitting Eq. (43) to the linear increase of the square of the frequency with pump power, we determine r at various compressions of the coils.

At ten different levels of applied cavity losses, the output light dynamics were documented over the available range of the pump. In particular, we are interested in the relative pump rate where sustained epochs of pulsing are first observed in the intensity. The results are shown in Fig. 6. For each level of cavity losses we recorded the pump rate associated with emergence of pulsing for eight sweeps of the diode pump. The diamonds in Fig. 6 plot the average onset point of pulsing. The standard deviation of the independent sweeps is smaller than the displayed symbol size.

For $-8 < \ln(r) < -6$ pulsing emerges close to lasing threshold near $x = 1.20$. The onset point rapidly climbs to larger pump rates for further increments of cavity losses, $\ln(r) < -8$, until pulsing is no longer observed. The persistence of the cw state at larger pump rates for increasing levels of cavity losses has previously been observed in a three-level Er-doped fiber laser [30].

The remaining model parameters of this laser system may be readily deduced. Using the stated fluorescence time for Nd-doped fiber and calculating the round-trip time from the cavity length, we find $\epsilon = 2.4 \times 10^{-4}$ for this laser. Measurements of the slope efficiency at different levels of cavity loss allow an estimation of the total linear gain G_{tot}. According to Eq. (40) the slope efficiency linearly decreases with a reduction of $\ln(r)$ (increasing cavity

losses) and reaches zero when the magnitude of $\ln(r)$ matches the total linear gain. The slope efficiencies measured from laser operation at various levels of applied cavity losses are plotted as squares in Fig. 7(b). The zero crossing of a linear fit to these points yields an estimate of $G_{tot} = 10.83$.

The Hopf bifurcation curve $x_H(r)$ is calculated from Eq. (41) to evaluate the onset of the pulsing regime predicted by the modified four-level model. This curve is represented in Fig. 6 by the solid line. For comparison, the dashed line shows the bifurcation curve predicted by the original model. For low and moderate cavity losses the two curves are almost indistinguishable; for larger cavity losses, decreasing $\ln(r)$, the two curves separate and the modified model predicts a higher threshold for the onset of pulsing, in good agreement with the experiments (diamonds). The dotted lines A_1 and A_2 in Fig. 6 bound the range of cavity losses where pulsing is predicted in the modified model.

V. DISCUSSION

The quantitative agreement between the iterative map computations and experiments suggests that, for each lasing scheme, the model contains a sufficient degree of physical detail to accurately reproduce the spectrum of dynamical states witnessed in fiber lasers. This feature is unique to the iterative map formulation, as the pulsing state is not readily reproduced in traditional rate equation descriptions containing the same physical considerations [31]. The absence of pulsing dynamics in the rate equations stems from an invocation of the slowly-varying wave approximation to deduce the differential equation for the electric field or intensity from the associated iterative map. Additional physical mechanisms have previously been added to the underlying rate equations to capture pulsing dynamics at low pump rates. These efforts include the incorporation of a coherence variable [31], ion-pair clusters in Er-doped fiber acting as a saturable absorber [32], and interaction between the pump and lasing fields [33].

Nevertheless, pulsing dynamics are often observed in a variety of high-gain fiber lasers even when no additional mechanism can be clearly identified. The pulsing state arises naturally in the iterative map model and the pump rate where pulsing dynamics emerge is highly dependent on the level of cavity losses and the total linear gain in the active medium. For both three-level and four-level lasing schemes, general features emerge when the system

is evaluated over a large range of total linear gain. When the cavity losses are very low or very high the system emits solely in the cw regime regardless of how high the system is pumped. Cavity losses falling between these extremes allow the emergence of the pulsing state when the pump strength is tuned beyond a bifurcation point close to lasing threshold. For small G_{tot} this point occurs at pump rates high above lasing threshold. The span of pump exhibiting stable cw emission narrows as the total linear gain is increased: in a four-level lasing scheme the onset of pulsing approaches the dotted line in Fig. 6, while in a three-level lasing scheme the onset point is pushed further down until it rests slightly above lasing threshold for all moderate levels of cavity losses.

In conclusion, we have refined an iterative map model describing fiber laser array dynamics to include a broad class of lasing schemes and operating conditions. These modifications expand the scope of the model to three-level and four-level lasers and remain valid even in the limit of cavity losses approaching the total linear gain of the system. Quantitative comparisons of steady state and transient dynamics reported in experiments demonstrate remarkable agreement with model predictions for both lasing schemes. Our results indicate that both cw and pulsing state dynamics are succinctly captured using only a few parameters commonly found in rate equation descriptions of the system. One strength of our approach is that these parameters may be estimated from accessible empirical measurements. The observations here may serve as guidelines in the selection of operating conditions for a broad class of fiber laser systems in order to achieve a desired dynamical behavior.

We thank Monica Minden for helpful discussions. This work was supported by the High Energy Laser Joint Technology Office and the US Army Research Office under Award No. W911NF-05-1-0506. Any opinions, findings, and conclusions or recommendations expressed in this publication are those of the authors and do not necessarily reflect the views of the High Energy Laser Joint Technology Office or the Army Research Office.

---

[1] H. Haken, Phys. Lett. **53A**, 77 (1975).

[2] P. Colet and R. Roy, Opt. Lett. **19**, 2056 (1994).

[3] G. VanWiggeren and R. Roy, Science **279**, 1198 (1998).

[4] G. VanWiggeren and R. Roy, Phys. Rev. Lett. **81**, 3547 (1998).

[5] R. Roy, T. Murphy, T. Maier, and Z. Gills, Phys. Rev. Lett. **68**, 1259 (1992).

[6] M. Todd, J. Nichols, L. Pecora, and L. Virgin, Smart Mater. Struct. **10**, 1000 (2001).

[7] L. Moniz, J. Nichols, S. Trickey, M. Seaver, D. Pecora, and L. Pecora, Chaos **15**, 023106 (2005).

[8] S. Wang and H. Winful, Appl. Phys. Lett. **52**, 1774 (1988).

[9] H. Winful and S. Wang, Appl. Phys. Lett. **53**, 1894 (1988).

[10] R. Roy and K. Thornburg, Jr., Phys. Rev. Lett. **72**, 2009 (1994).

[11] T. Heil, I. Fischer, W. Elsässer, J. Mulet, and C. Mirasso, Phys. Rev. Lett. **86**, 795 (2001).

[12] J. Terry, K. Thornburg, Jr., D. DeShazer, G. VanWiggeren, S. Zhu, P. Ashwin, and R. Roy, Phys. Rev. **E 59**, 4036 (1999).

[13] J. Sharpe, P. Ramazza, N. Sungar, and K. Saunders, Phys. Rev. Lett. **96**, 094101 (2006).

[14] F. Arecchi, G. Giacomelli, P. Ramazza, and S. Residori, Phys. Rev. Lett. **65**, 2531 (1990).

[15] I. Fischer, R. Vicente, J. Buldú, M. Peil, C. Mirasso, M. Torrent, and J. García-Ojalvo, Phys. Rev. Lett. **97**, 123902 (2006).

[16] D. Botez and D. Scifres, eds., *Diode Laser Arrays* (Cambridge University Press, 1994).

[17] H. Bruesselbach, M. Minden, J. Rogers, D. Jones, and M. Mangir, in *2005 Conference on Lasers and Electro-Optics (CLEO)* (2005), vol. 1, p. 532.

[18] N. Lyndin, V. Sychugov, A. Tikhomirov, and A. Abramov, Quantum Electron. **24**, 1058 (1994).

[19] V. Kozlov, J. Hernández-Cordero, and T. Morse, Opt. Lett. **24**, 1814 (1999).

[20] A. Shirakawa, T. Saitou, T. Sekiguchi, and K. Ueda, Opt. Exp. **10**, 1167 (2002).

[21] T. Simpson, A. Gavrielides, and P. Peterson, Opt. Exp. **10**, 1060 (2002).

[22] H. Bruesselbach, D. Jones, M. Mangir, M. Minden, and J. Rogers, Opt. Lett. **30**, 1339 (2005).

[23] A. Siegman, URL ⟨`http://www.stanford.edu/~siegman/coupled_fiber_modes.pdf`⟩.

[24] E. Bochove, P. Cheo, and G. King, Opt. Lett. **28**, 1200 (2003).

[25] J. Rogers, S. Peles, and K. Wiesenfeld, IEEE J. Quantum Electron. **41**, 767 (2005).

[26] E. Lacot, F. Stoeckel, and M. Chenevier, J. Phys. III France **5**, 269 (1995).

[27] R. Böhm, V. Baev, and P. Toschek, Opt. Comm. **134**, 537 (1997).

[28] A. Siegman, *Lasers* (University Science Books, 1986).

[29] C. Millar, I. Miller, B. Ainslie, S. Craig, and J. Armitage, Electron. Lett. **23**, 866 (1987).

[30] P. Le Boudec, M. Le Flohic, P. Francois, F. Sanchez, and G. Stephan, Opt. Quantum Electron.

25, 359 (1993).

[31] E. Lacot, F. Stoeckel, and M. Chenevier, Phys. Rev. **A 49**, 3997 (1994).

[32] F. Sanchez, P. Le Boudec, P. Francois, and G. Stephan, Phys. Rev. **A 48**, 2220 (1993).

[33] L. Luo and P. Chu, Opt. Comm. **135**, 116 (1997).

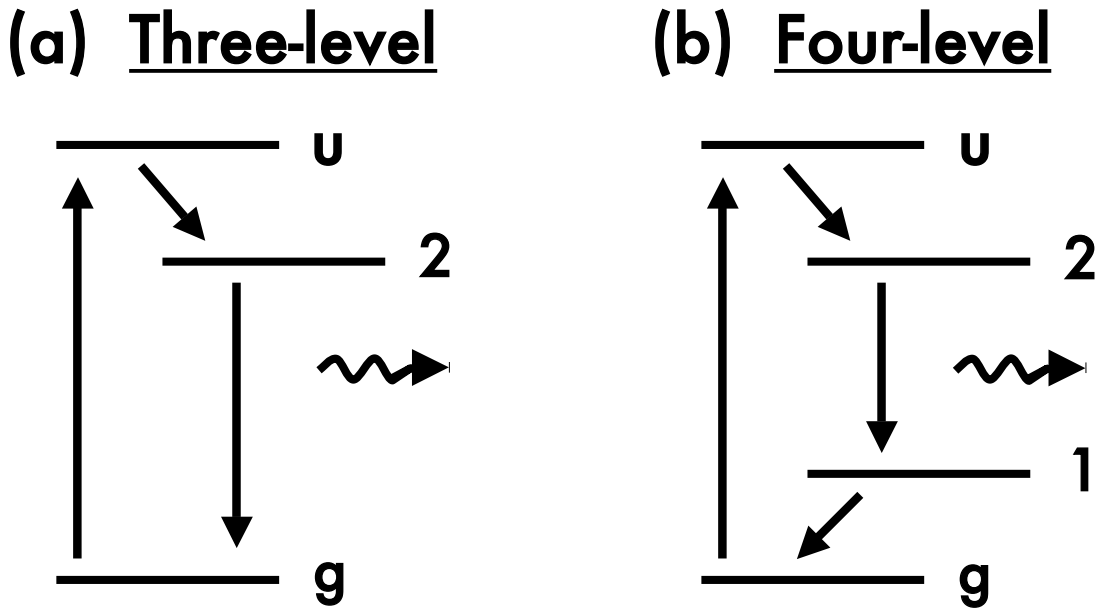

FIG. 1: Energy levels involved in the (a) three-level and (b) four-level lasing scheme. In (a) inversion is defined by the population difference between levels 2 and g and in (b) between levels 2 and 1.

TABLE I: Three-level laser parameters from Ref. [26]

Cavity length $L\ (m)$	Amplification rate $N_{tot}B'\ (s^{-1})$	Pump absorption coefficient $C^p\ (s^{-1}mW^{-1})$	Cavity decay time $T_{cav}\ (s)$
3	1.84×10^8	7.84	6.33×10^{-9}
4	1.84×10^8	7.12	6.61×10^{-9}
4.5	1.84×10^8	6.87	7.06×10^{-9}

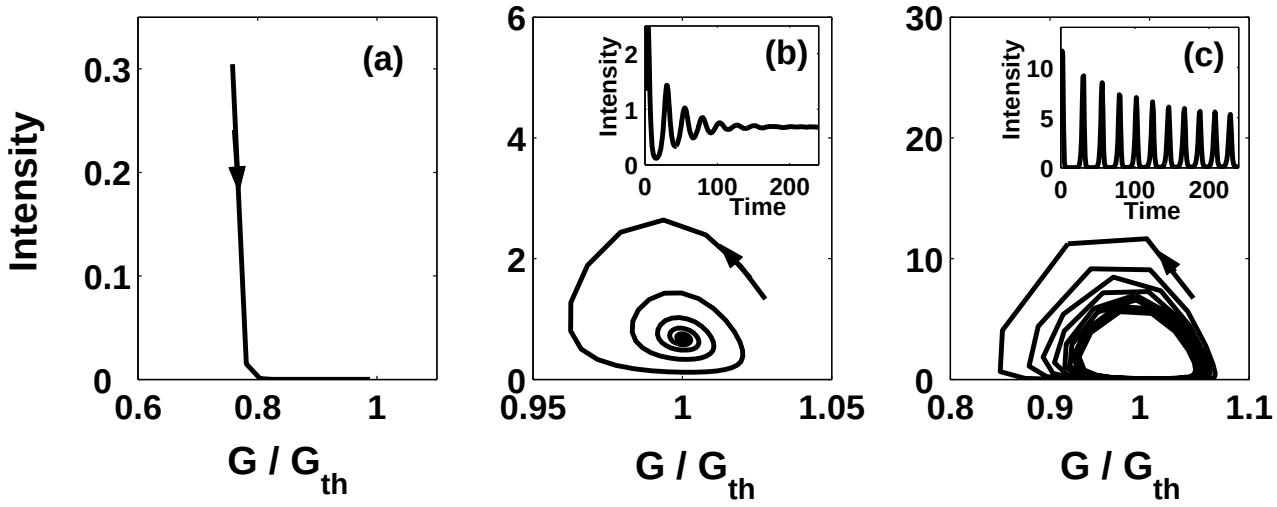

FIG. 2: System trajectory in the scaled I and G phase portrait for decay of transient towards (a) off state with $W^p/W^p_{th} = 0.98$, (b) cw state with $W^p/W^p_{th} = 1.10$, and (c) pulsing state with $W^p/W^p_{th} = 1.18$. Inset panels of (b) and (c) plot the intensity time trace associated with each phase portrait.

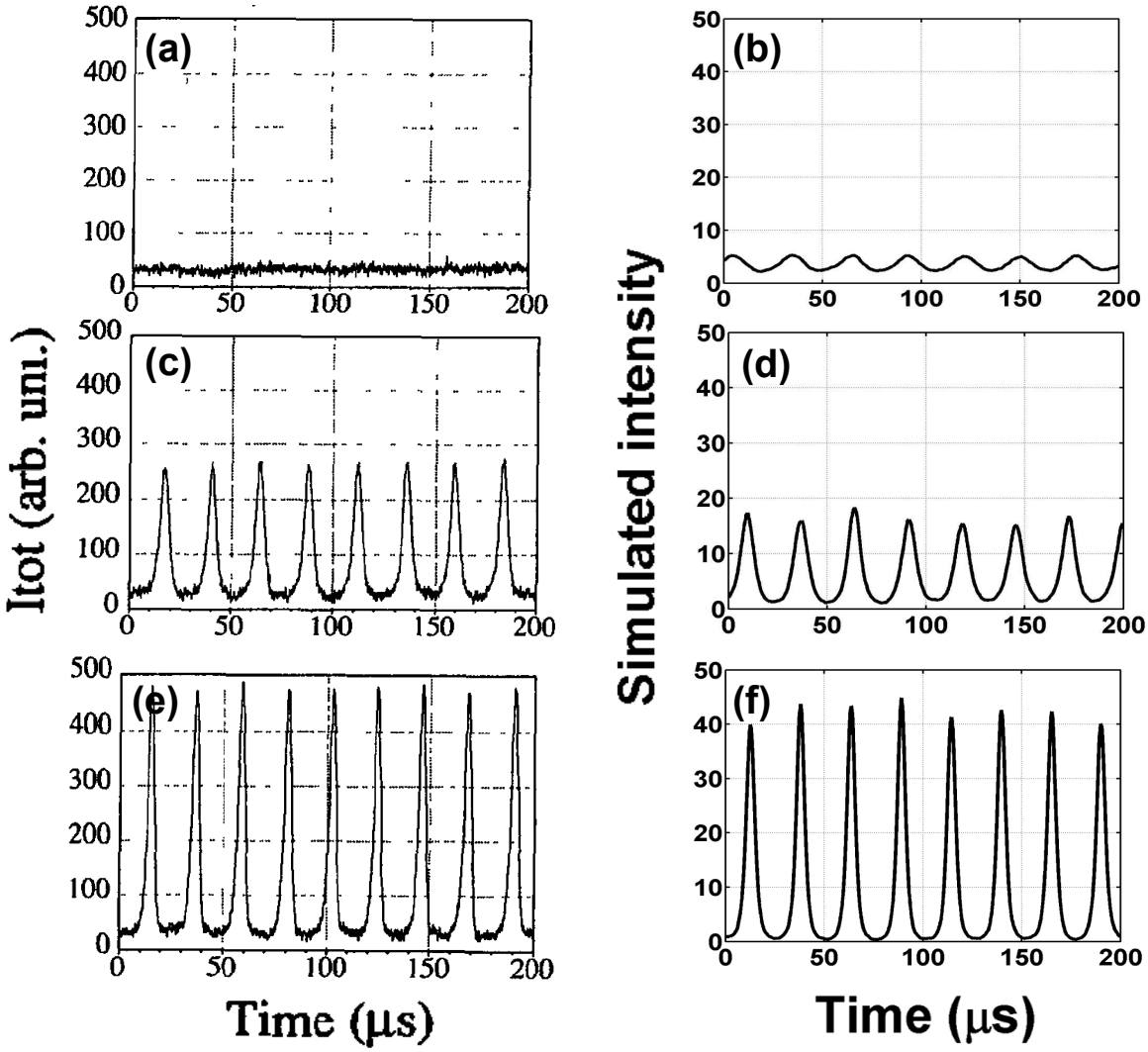

FIG. 3: Comparison of previously reported experiments and simulations of Eqs. (23) and (24). Left column is a reproduction of Fig. 6 in Ref. [26] showing experimental intensity time series for (a) 3m, (c) 4m, and (e) 4.5m cavity length for the same amount of pumping. Intensity time series computed from the model using parameters in Table I for (b) 3m, (d) 4m, and (f) 4.5m cavity length.

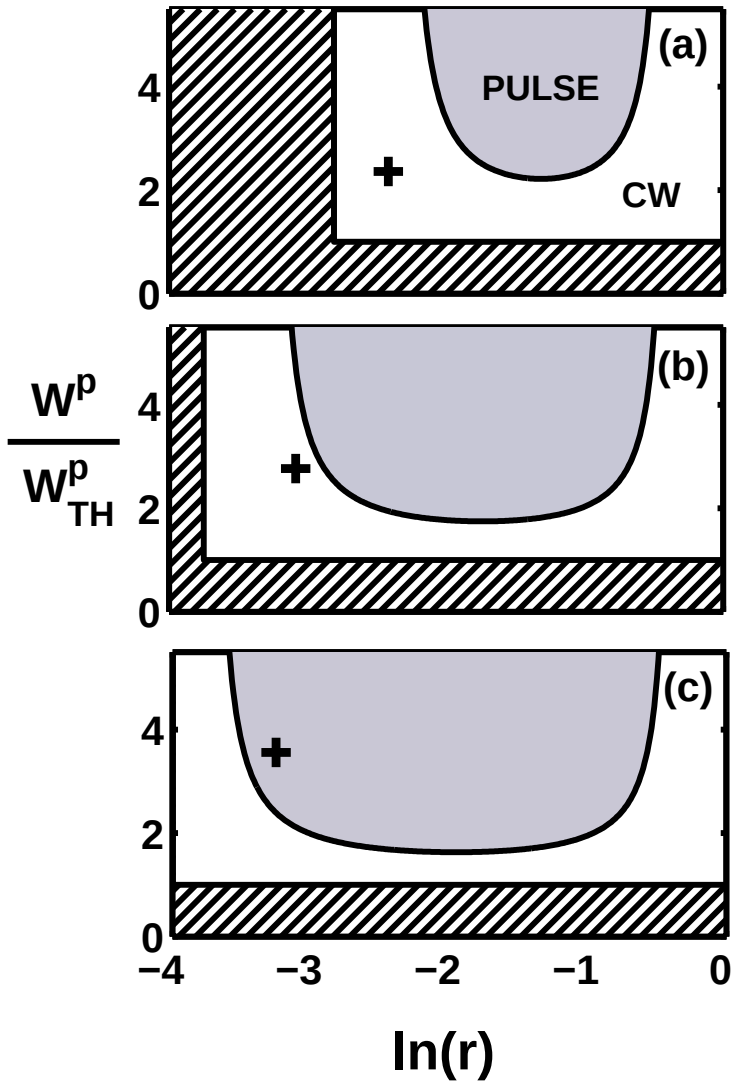

FIG. 4: Steady state dynamics predicted by Eqs. (23) and (24) using empirically derived G_{tot} from Ref. [26] for (a) 3m, (b) 4m, and (c) 4.5m cavity length. The cross-hatched region denotes the off state, the white region corresponds to stable cw emission, and the gray region plots the parameter range for pulsing dynamics. The cross in each panel signifies the operating conditions of the simulated intensity time series respectively shown in Fig. 3(b), (d), and (f).

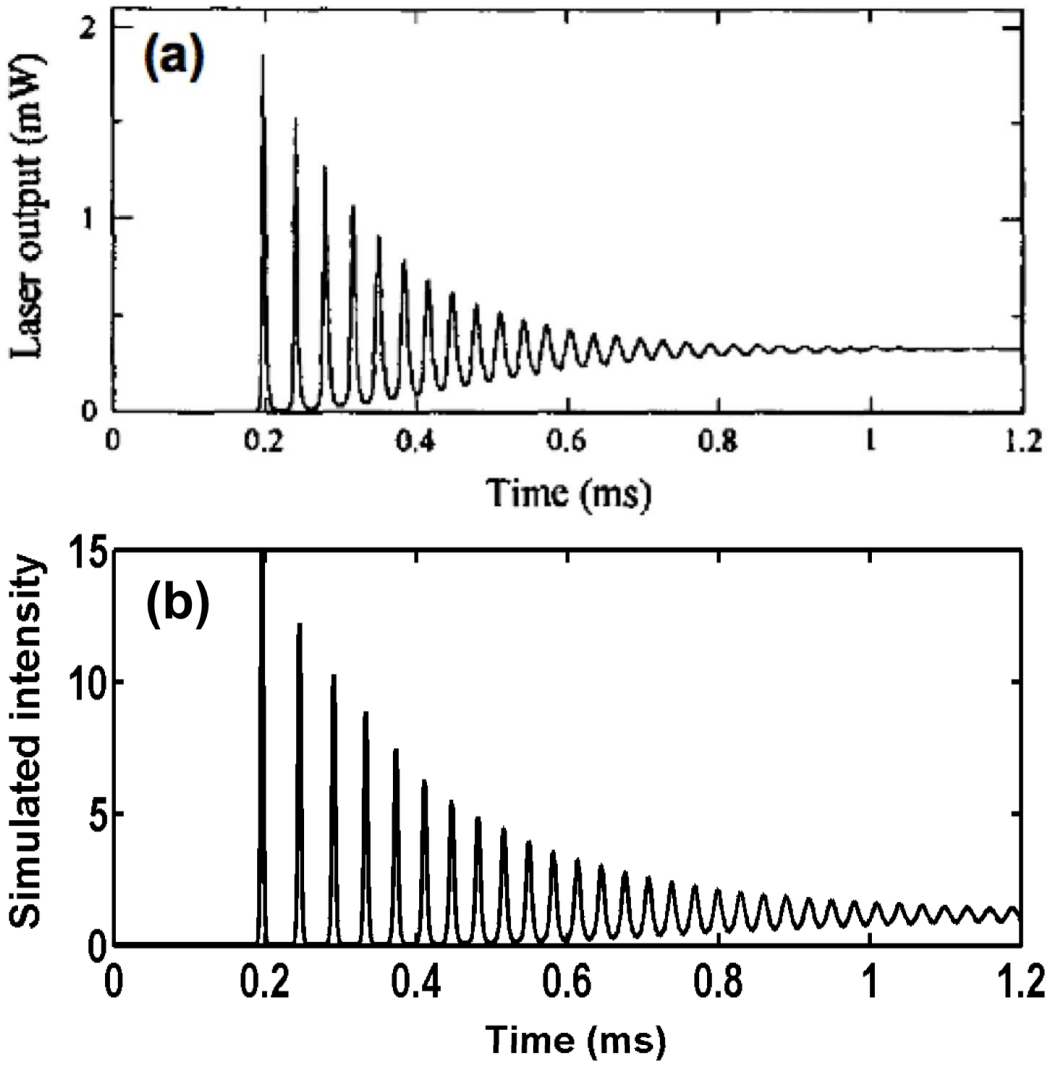

FIG. 5: Intensity time series after pump is switched on at time zero. (a) Reproduction of Fig. 4 in Ref. [27] showing experimental time trace. (b) Simulated intensity time series from iterative map model.

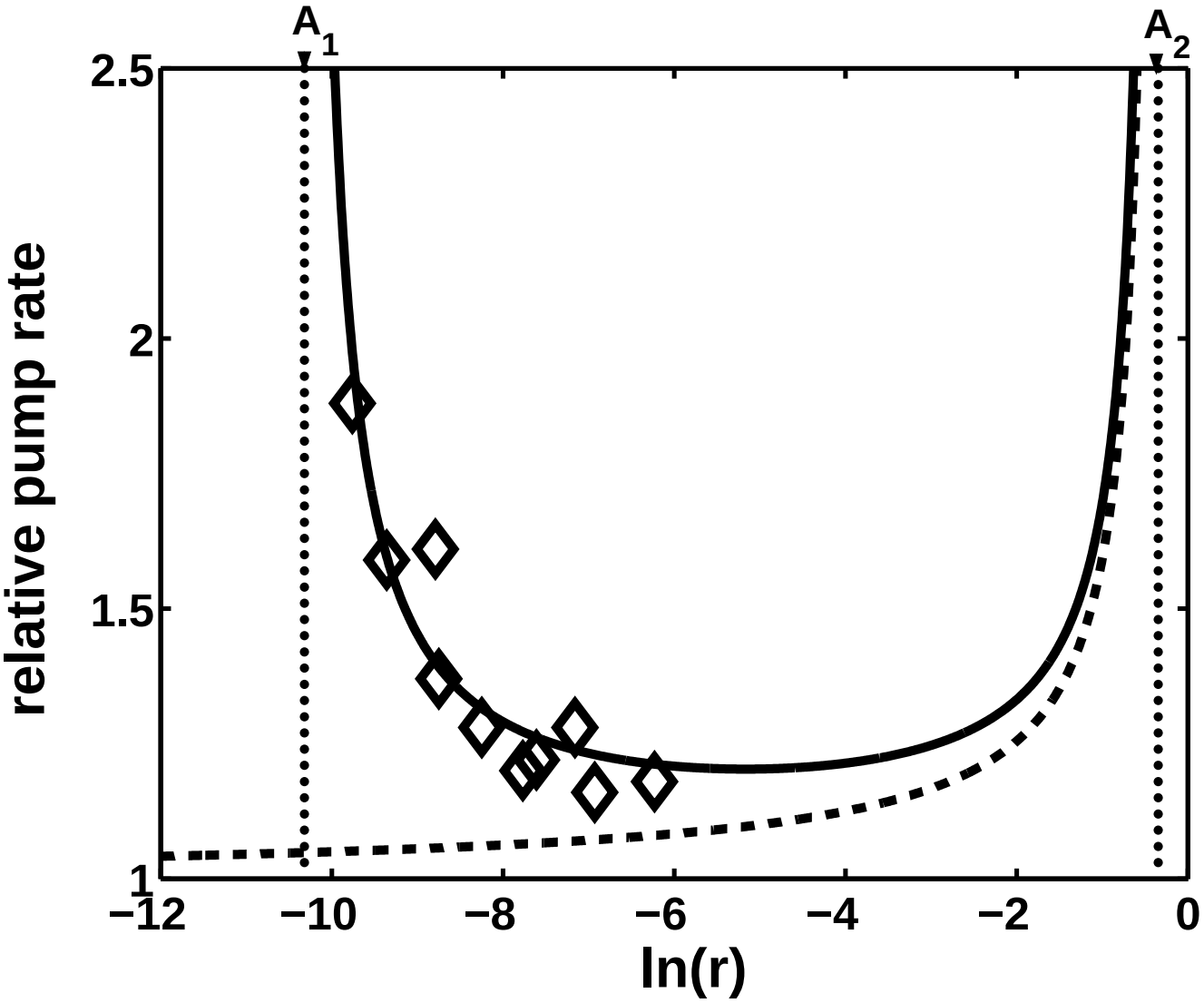

FIG. 6: Hopf bifurcation curve separating cw and pulsing emission is calculated for four-level modified map with $G_{tot} = 10.83$ (solid line) and for original map (dashed line). The vertical dotted line A_1 and A_2 represent asymptotes of modified map bounding the range of cavity losses where pulsing is predicted. The diamonds denote experimentally measured onset points of pulsing in our new 4-level experiments.

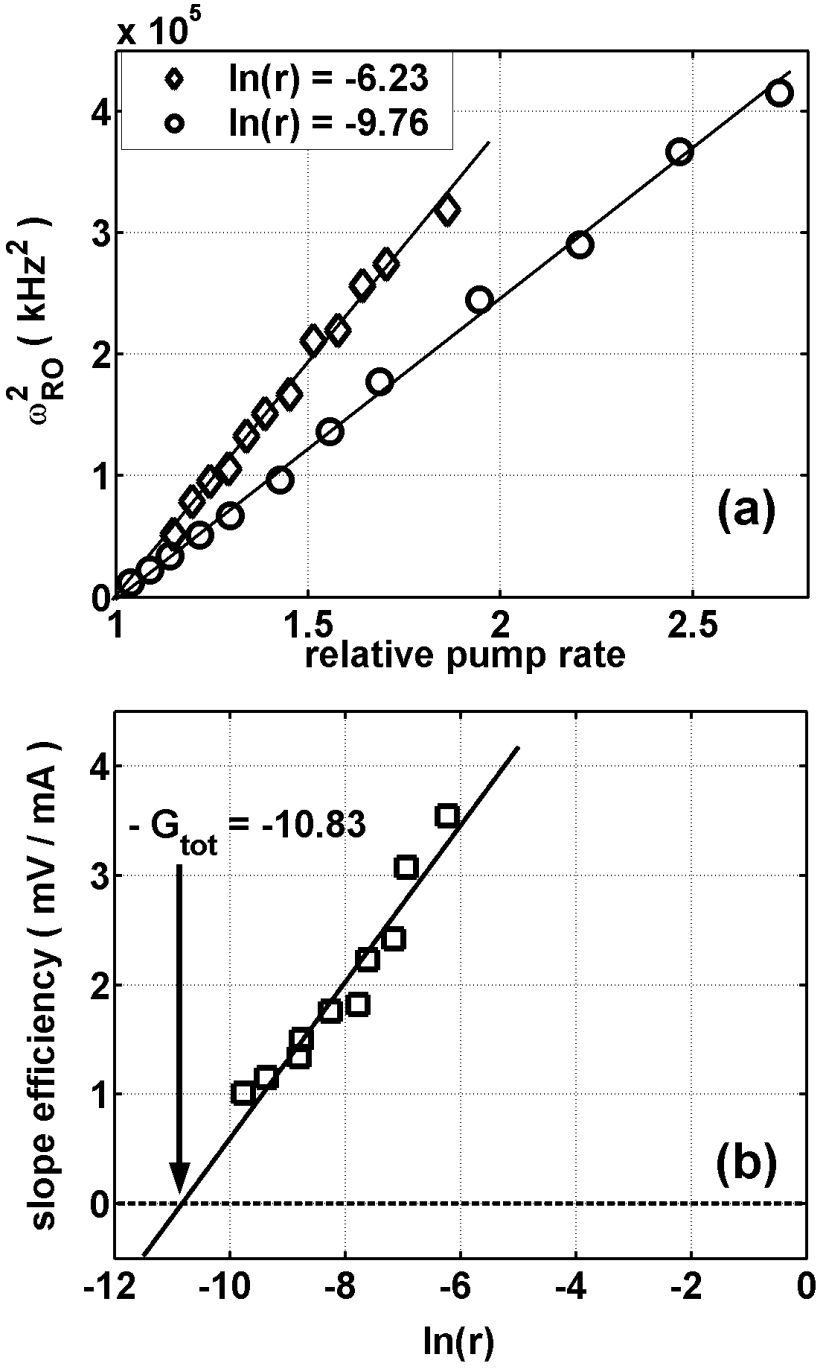

FIG. 7: Experimental measurements from our experiments on Nd-doped fiber lasers. (a) Square of frequency of relaxation oscillations for cavity losses $\ln(r) = -6.23$ and $\ln(r) = -9.76$. (b) Slope efficiency determined at ten levels of cavity losses. The zero crossing of the linear fit yields an estimation of $G_{tot} = 10.83$.

TABLE II: Correspondence between parameters of the iterative map model and the empirical measurements shown in Table I. The reported parameters include the cavity decay time T_{cav}, the product of the total population and Einstein coefficient $N_{tot}B'$, the length of the cavity L, and the pump absorption coefficient C^p. The expressions include constants for the speed of light c, the index of refraction η in the fiber, and the input power P from the pump source.

Iterative map model	Reported measurement	Relationship
r	T_{cav}	$r = e^{-\frac{L\eta}{cT_{cav}}}$
G_{tot}	$N_{tot}B'$	$G_{tot} = \frac{L\eta}{c}\left(N_{tot}B'\right)$
T	L	$T = \frac{2L\eta}{c}$
W^p	C^p	$W^p = C^p P$